

Determination of physical properties of CSP materials under concentrated solar irradiation

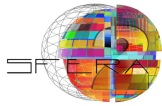
Characterization of the physical and chemical properties of the surface of cavities of porous materials

SFERA II Project	
Solar Facilities for the European Research Area -Second Phase	
Grant agreement number:	312643
Start date of project:	01/01/2014
Duration of project:	48 months
WP13 – Task 1.A	Deliverable 13.6
Due date:	12/2015
Submitted	08/2016
File name:	WP13 – Task 3.A Deliverable 13.6
Version	1.0
Partner responsible	CNRS
Person responsible	Eric Beche
Author(s):	Eric Beche
Dissemination Level	PU



List of content

1) Abstract.....	4
2) Introduction	4
3) Experimental	7
4) Results and discussion: XRD analysis	10
5) Results and discussion: XPS analysis	13
5.1) Qualitative and quantitative depth profiles (SiC foam)	14
5.2) Qualitative and quantitative depth profiles (ZrB ₂ foam).....	18
6) Conclusions	21
7) References	24



Executive Summary

The EU-funded research project SFERA2 – grant agreement 312643 – aims to boost scientific collaboration among the leading European research institutions in solar concentrating systems, offering European research and industry access to the best research and test infrastructures and creating a virtual European laboratory.

This deliverable is part of the results of the task 3 of the workpackage 13 *Determination of physical properties of CSP materials under concentrated solar irradiation* within the Joint Research Activities.

This workpackage 13 aims to provide a better evaluation of the material behavior for CSP applications and other fields with similar thermal stress, such as high temperature steels or SiC, ZrB₂ ceramics, thanks to better or new experimental tests bed and associated theoretical models. These results will lead to help users developing higher performance materials for higher process efficiency.

The task 3 of workpackage 13 is focused on 2 principal targets:

- Adaptation of methods to characterize physical and chemical surface properties inside the cavities of porous materials to determine the real history and modifications of the material after use in CSP applications.
- Evaluation of transfer properties of porous materials both experimentally with upgraded solar test bed and theoretically with improved numerical methods.

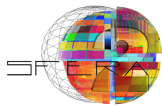
The work presented, related to the first task 3 target, here focus on the selection of two analytical techniques (X-Ray Diffraction and X-Ray Photoelectron Spectroscopy) to validate methods for the characterization of walls of the cavity foams. This selection is made by studying the evolution of the chemical composition and environments of virgin and treated samples (SiC and ZrB₂ foams).

In an introduction, the oxidation process of SiC and ZrB₂ foams is presented. Then, the solar facility and experimental setup are summarized. The analytical techniques and methods and the selected samples are then presented.

The XRD analysis were carried out in order to observe the modifications of crystalline phases after a heating treatment and to first select promising candidate for CSP applications.

The XPS analysis were carried out in order to determine the chemical environment, the nature of the chemical bonds, and the chemical composition from the surface to the substrate for heated samples (SiC and ZrB₂ foams). The presentation of the parameter optimization was required to allow the reader to understand which variables are needed to be studied to analyze no-flat and small surfaces (< 0.1 mm²) of cavity wall.

The discussion about XPS results is followed by this work conclusion.



1) Abstract

This study concerns the characterization of the surface cavities of porous materials as ceramics foams used in high temperature volumetric solar absorbers. These ceramics materials must reach high efficiency at high temperature. Several foam samples currently available in the industry were characterized by XRD (Aluminium oxide: Al_2O_3 , Zirconium oxide: ZrO_2 and silicon carbide: SiC). However, Al_2O_3 and white ZrO_2 compounds revealed low solar absorptivity efficiency for thermo solar conversion⁽¹⁾. Experimental results obtained for SiC foams (measured absorptivity = 0.7-0.8, IR-TF SOC 100)⁽²⁾, considered to be the reference material for volumetric absorber. New selective foam (Zirconium diboride, ZrB_2) with spectral selectivity i.e. high solar absorptivity (0.7 to 0.8) and low infra-red emissivity was first investigated by XRD. Experimental methods for XPS were optimized in order to characterize the wall of the pores. XPS could become one of the most appropriate techniques to analyze oxidized foams (surface and bulk). After a heating treatment with solar energy, the microstructure (crystalline phases, chemical bonds and environments, chemical composition...) and the oxidation behavior of the ZrB_2 and SiC foams were determined.

Keywords: XPS, XRD, high temperature, oxidation process, ceramic foams

2) Introduction

SiC compounds have been developed into a high quality technical grade ceramic with very relevant properties for volumetric solar absorbers. Under heating treatment in air, a protective silicon oxide coating is formed from 1500 to about 1850 K. High thermal conductivity and low thermal expansion coefficient, high strength are key properties for thermal shock resistances. Chemical purity of silicon carbide ceramics leads to high strength close to 1900 K. Other interesting properties are low density, high hardness and fracture toughness, high elastic modulus⁽³⁾. SiC compounds have several crystallographic phases (cubic (β - SiC), rhombohedral and hexagonal (α - SiC)) with more than 170 polytypes with two identical dimensions and a different third. During a heating treatment in air (atmospheric pressure), the α - SiC phase is thermodynamically more stable than the β - SiC phase.

The microstructure of surface and the properties of materials heated at high temperature with solar energy depend of the oxidation behavior and process. SiC compounds are oxidized following two regimes mainly depending on the oxygen partial pressure, the temperature of treatment and the crystalline phase of SiC layer. Several authors studied the oxidation process of SiC materials⁽⁴⁻³³⁾ and two reviews about the oxidation process of SiC have been recently written by Roy et al⁽³⁴⁾ and Jacobson et al⁽³⁵⁾.



The passive oxidation process often occurs at low temperature (above 900 K) and high partial pressure of oxygen. This process leads to the formation of a protective, homogenous and dense layer of silica on the surface of SiC compound. A mass increase is observed. Our previous studies of kinetic oxidization at different temperatures (1700 to 1900 K) vs times of oxidation, on CVD β -SiC samples^(36,37) revealed two analytical models described by parabolic and linear curves. The parabolic process is limited by the diffusion of oxygen atoms through the silica layer. The second process mainly depends of the chemical reactions^(34,38-43).

The passive oxidation reactions of a SiC layer are described by:



or



In contrast, the active oxidation process occurs at high temperature and low partial pressure of oxygen ($< 1.10^5$ Pa). This process reduces the strength and leads to mass loss of the sample. The SiC layer is not protected and gradually destroyed with SiO and CO gas species emissions. The active oxidation reaction of a SiC layer is described by:



or

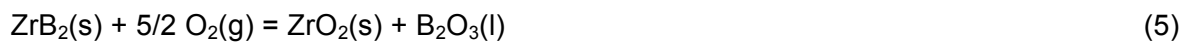


At the passive-active transition, five compounds or species can be detected with two solid phases SiC(s), SiO₂(s) and one gas phase composed by O₂(g), CO(g), SiO(g). The parameters of this system are the total pressure, the temperature and the oxygen partial pressure. So, the variance of this system is three. For the passive/active transitions oxidation regime, Balat⁽⁸⁾ and Presser et al⁽⁴⁴⁾ present a critical review of theoretical or experimental data, according to the partial pressure of oxygen species and the temperatures. The variety of reported experimental results can be explained by the nature of the silicon carbide specimen (polytypes, microstructure, chemical composition, purity, grain size, grain boundary, density impurities or sintering aids contents), the gas flow, the partial and total pressures, the method used and the criterion taken to define the transition. Experimental transitions of the mixed process (passive/active and active/passive) were studied by other authors^(28,30,31,35,39,45,46).



Ceramic compounds based on metal borides, such as zirconium diboride (ZrB_2) are defined as UHTCs because of their high melting temperatures, which are greater than 3300K. ZrB_2 materials have a lower theoretical density (6.09 g/cm^3), high thermal conductivity, high hardness which classifies them as promising candidates in several industrial sectors in particularly for high temperature volumetric solar absorbers. The value of the fracture toughness in ZrB_2 ceramics is approximately $3.8 \text{ MPa}\cdot\text{m}^{1/2}$. Many studies of ZrB_2 oxidization were carried out in order to show the oxidation resistance to a heating treatment and to understand the mechanisms and the modification of the chemical - physical properties of the layers ⁽⁴⁷⁻⁶²⁾.

Oxidation of ZrB_2 compounds leads to the formation of B_2O_3 and ZrO_2 oxides. The oxidation reactions of a ZrB_2 layer are described by:



and



B_2O_3 compound has a low melting point, close to 450°C . below 1100°C , a liquid phase of boria is formed and provides a glassy protective layer which reduced the oxygen diffusion through the zirconia layer (ZrO_2) to the diboride substrate layer (ZrB_2) The porous ZrO_2 structure is filled by the liquid B_2O_3 increasing the protective properties against oxidation of the diboride substrate. Several models of ZrB_2 compounds are reported by Parthasarathy et al ⁽⁵²⁾. Above 1100°C , the diboride zirconium is rapidly oxidized because of a rapid diffusion of oxygen through the ZrO_2 layer to the substrate. The rate of vaporization of the liquid B_2O_3 rapidly increases with increasing the heating treatment because of B_2O_3 has a high vapor pressure. According to Talmy et al ⁽⁶³⁾, about 15 % of boria can be detected within the oxide layer. The higher resistance of ZrB_2 layer could be explained by this residual presence of $B_2O_3(l)$. According to several studies ^(57,63,64) and our previous work ⁽⁵⁸⁾, ZrB_2 -SiC compounds revealed high oxidation resistance up to 1800 K. A protective layer of borosilicate compound was formed at the surface. The vaporization of B_2O_3 is stopped: boria compounds are enclosed in a borosilicate matrix. So, this glass presents higher melting temperature and lower oxygen diffusion than the B_2O_3 glass.

In summary, below 1100°C , the kinetic curve shows a parabolic behavior and above 1400°C , the curve is a linear contribution. In the range of 1100°C to 1400°C , the kinetic curve shows an intermediate shape ^(51,53,57,65).



In previous study⁽²⁾, several foam samples, currently available in industry, were tested in order to quantify the solar-to-thermal energy efficiency. These samples were investigated by XRD. Porosity and PPI values are in the range of 72-92 % and 5-20 PPI, respectively. According to the XRD results, to measured absorptivity values and to previous studies of ZrB₂ ceramics (spatial applications⁽⁵⁸⁾), SiC foams and a new candidate of ZrB₂ foam were selected in this work (EngiCer manufacturer).

This study focuses on the oxidation of silicon carbide (β -SiC) and diboride zirconium (ZrB₂) foams heated at high temperature with solar energy. The microstructure of the cavity surfaces of virgin and heated β -SiC and ZrB₂ foams were studied by XRD; the chemical and crystalline data provide from several cavities (1 or 2 pores). The main challenge is to analyze the microstructure of the surface of one cavity with a small X-ray beam ($0.15 \text{ mm} < \varnothing < 0.02 \text{ mm}$) in order to determine the chemical composition and the nature of the chemical bonds of atoms. One of the most appropriate techniques is the X-ray Photoelectron Spectroscopy (XPS). Understanding the chemical environment of the surface and in the bulk is necessary to explain the surface properties and the phenomena regulating the surface oxidation of these UHTC materials.

3) Experimental

Solar facility, experimental setup (Fig. 1 and 2):

The foam samples were heated in a 6 kW solar reactor (glass reactor). There were positioned at the focus of the concentrated solar radiation. The sample is surrounded by an alumina ring in order to avoid air leaks inside the device. The surface of the foam is heated by solar energy and the blown air is heated by convection through the ceramic foam. The temperature of the air flow was measured with 4 K-type thermocouples fixed at different points. The measurement of the equivalent blackbody temperature of the irradiated surface (ceramic foam) was performed using an IR camera (FLIR SC 1000). The experimental setup and the sample testing device were fully detailed⁽²⁾.

All the ceramic foams were tested under solar irradiation for about 30 min. The values of temperature of inlet and outlet air flow, $T_{f,in}$ (cold air) and $T_{f,out}$ (hot air) were in the range of 283 to 287 K and 1120 to 1180 K, respectively. The calculated temperatures of surface were about 1900 K. All the experimental conditions were summarized in ref. (2).

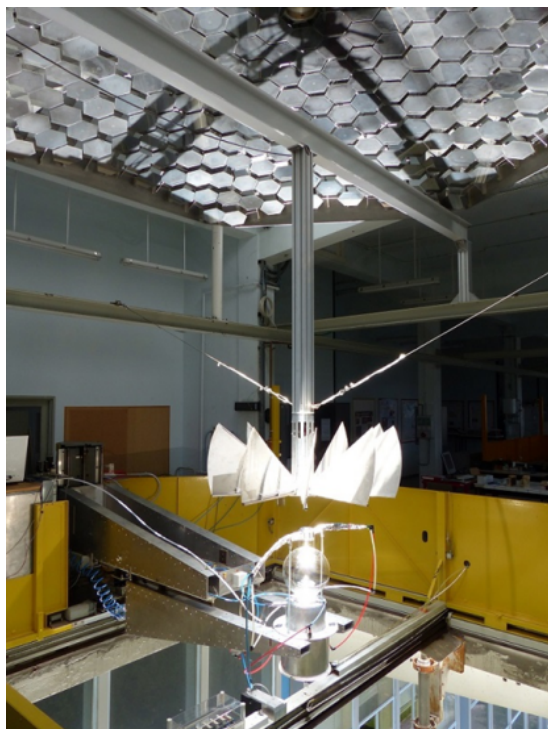


Figure 1: 6 kW solar furnace experimental setup

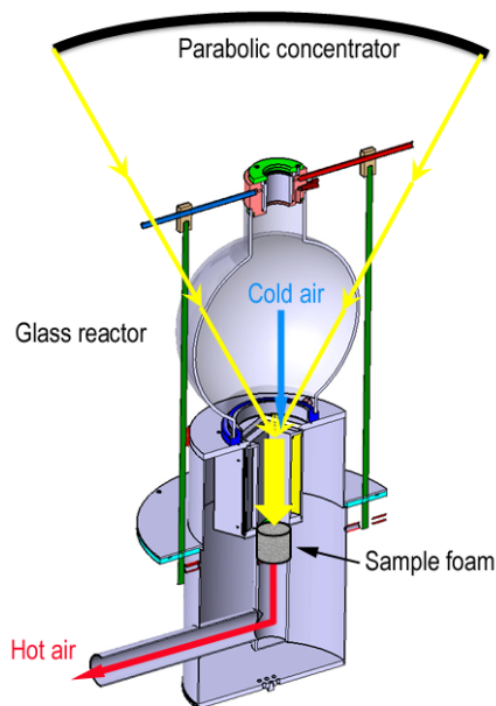


Figure 2: Solar reactor device (OPTISOL) ⁽²⁾

Analytical techniques:

XRD analyses were performed at room temperature using a PANalytical XPert Pro diffractometer (CuK α radiation, $\lambda = 0.15418$ nm). X-ray diffraction measurements of θ - θ symmetrical scans were made over an angular range of 10 to 100°. The step size and the time per step were fixed at 0.01° and 20 s, respectively. The X-ray diffractograms were recorded and studied using PANalytical softwares (Datacollector and HighScorePlus). The contribution from AlK α_2 was removed (Rachinger method⁽⁶⁶⁾). The instrumental function was determined using a reference material (SRM 660, lanthanum hexaboride, LaB₆ polycrystalline sample) and can be expressed by a polynomial function.

XPS analyses were performed using a Thermoelectron ESCALAB 250 device. The photoelectron emission spectra were recorded using Al-K α radiation ($h\nu=1486.6$ eV) from a monochromatised source. The analysis area was approximately 0.015mm². The pass energy was fixed at 20 eV. The spectrometer energy calibration was made using the Au 4f_{7/2} (83.9 ± 0.1 eV) and Cu 2p_{3/2} (932.8 ± 0.1 eV) photoelectron lines. XPS spectra were recorded in direct N(E_c). The background signal was removed using the Shirley method⁽⁶⁷⁾. The atomic concentrations were determined with an accuracy less than 10 % from photoelectron peak areas using the atomic sensitivity factors reported by Scofield⁽⁶⁸⁾, taking into account the transmission function of the analyser. This function was calculated at different pass energies from Ag 3d and Ag MNN peaks collected for a silver reference sample. The binding energy scale was established by referencing the C 1 s value of adventitious carbon (284.8 eV ± 0.1



eV). The photoelectron peaks were analysed by Gaussian/Lorentzian (G/L = 50) peak fitting. The fixed full-width at half-maximum (FWHM) and the fixed positions of the components were similar to those collected for the reference samples.

Sample description:

The nature of the samples is reported in table 1. The visual identification of the samples (virgin and treated) is shown tables 2 and 3. For several samples, the requested information about microstructure provided by the manufacturer is poor. So, microstructural analyses were necessary to complete the identification card of foams. The microstructure of the cavity surfaces of virgin and heated foams were first studied by XRD; the chemical and crystalline informations provide from 1 to 4 cavities, depending of the pore sizes. The sample size is 5 cm (diameter) by 4 cm (height).

Samples	Description of the samples
Al ₂ O ₃	Al ₂ O ₃ , 20 ppi, Canada
ZrO ₂	ZrO ₂ , 20 ppi, Canada
SiC01	SiC, 40 ppi, China
SiC02	SiC, 20 ppi, Canada
SiC03	SiC,5 ppi, LANIK manufacturer, Czech Republic
SiC04	Si-SiC, 15 ppi, EngiCer manufacturer, Switzerland
SiC05	CVD-SiC coating / Si-SiC, 20 ppi, EngiCer manufacturer, Switzerland
ZrB ₂	Si-ZrB ₂ , 20 ppi, EngiCer manufacturer, Switzerland

Table 1: Identification of the ceramic foams



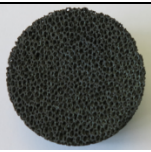
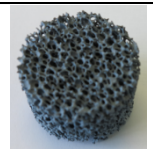

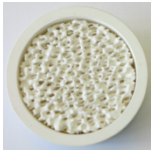

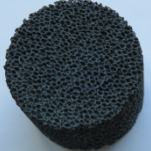
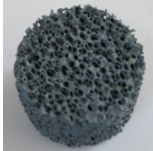

	Al ₂ O ₃	ZrO ₂	SiC01	SiC02	SiC03
Virgin samples					
Heated samples					

Table 2: Identification of the ceramic foams: Al₂O₃, ZrO₂, SiC01, SiC02, SiC03.

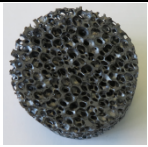
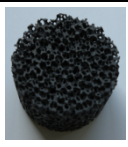
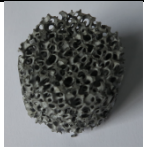
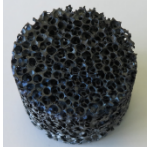

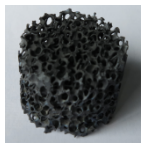
	SiC04	SiC05	ZrB ₂
Virgin samples			
Heated samples			

Table 3: Identification of the ceramic foams (EngiCer manufacturer): SiC04, SiC05, ZrB₂.

4) Results and discussion: XRD analysis

The XRD analyses were also carried out in order to observe the modifications of crystalline phases after a heating treatment.

The XRD patterns collected for initial and heated Al₂O₃ and ZrO₂ samples are shown in figures 3a and 3b. The diffractograms collected for the Al₂O₃ foams are attributed to Al₂O₃ crystalline phase (corundum, JCPDF 75-1862, rhombohedral system, R-3c space group (167)). The diffractograms collected for the ZrO₂ foams are attributed to ZrO₂ crystalline phase (JCPDF 83-0940, monoclinic system, P21/c space group (14)).

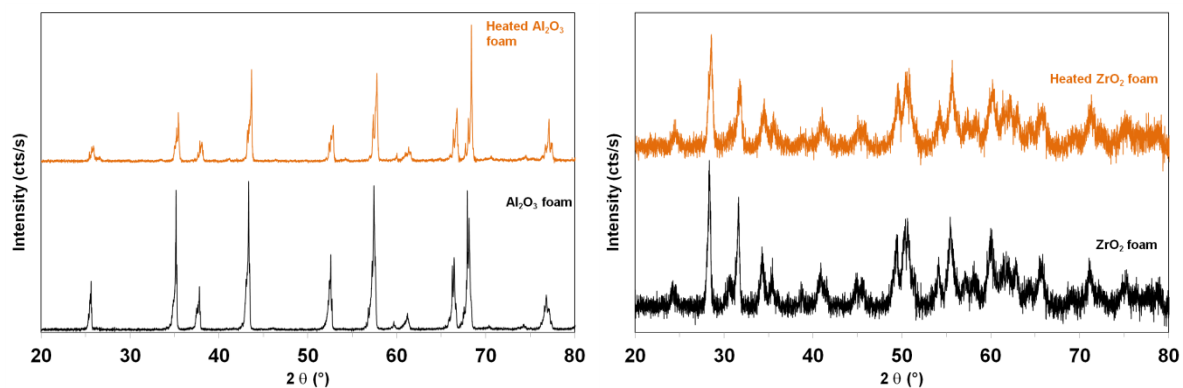
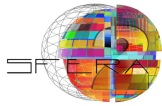


Figure 3: Diffraction patterns collected for no-heated and heated Al₂O₃ (3a) and ZrO₂ (3b) foams.

The XRD patterns collected for initial and heated sample SiC01 are shown in figure 4 (left).

The diffractogram collected for SiC01 foam (fig.4) is attributed to a α -SiC phase (triangle) Moissanite-6H, JCPDF 74-1302, Hexagonal system, P63mc space group (186)).

For heated SiC01 foam, minor SiO₂ phase (round) was detected (alpha low cristobalite, JCPDF 76-0941, tetragonal system, P41212 space group (92)). The surface of the SiC foam was oxidised. The main crystalline phase still remains a α -SiC compound. The minor Si peaks (square) could provide from infiltrated Si in the SiC compound (JCPDF 71-4631, cubic system, Fd-3m space group (227)).



The XRD patterns collected for initial and heated samples SiC02 are shown in figure 5 (right). Similar results were observed for diffraction patterns collected for sample SiC03 (not presented). The diffractograms collected for SiC02 foams are attributed to a α -SiC phase (triangle) Moissanite-6H, JCPDF 74-1302, Hexagonal system, P63mc space group (186). However, two oxide crystalline phases were also detected for virgin samples:

- Al_2O_3 crystalline phase (diamond, corundum, JCPDF 71-1127, rhombohedral system, R-3c space group (167)).
- SiO_2 crystalline phase (round, alpha low cristobalite, JCPDF 76-0941, tetragonal system, P41212 space group (92)).

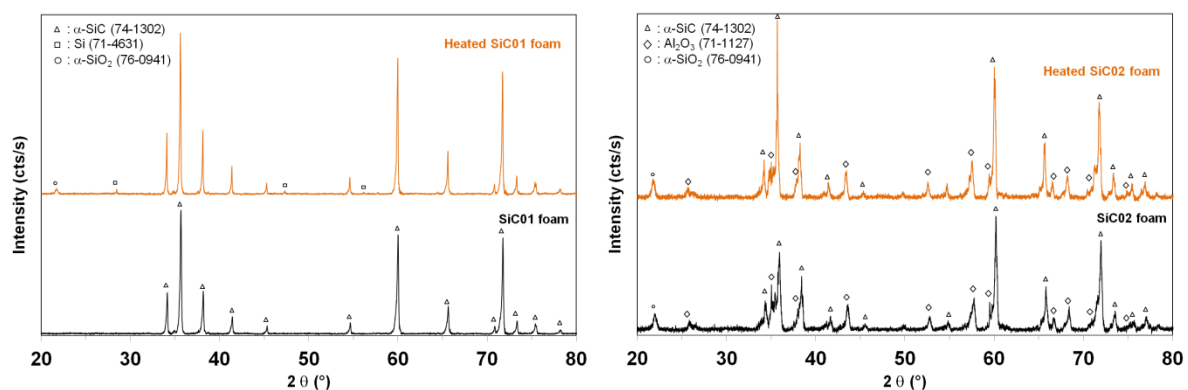


Figure 4 (left): Diffraction patterns collected for no-heated and heated sample SiC01: α -SiC (triangle), α - SiO_2 (round) and Si (square)

Figure 5 (right): Diffraction patterns collected for no-heated and heated sample SiC02: α -SiC (triangle), Al_2O_3 (diamond) and α - SiO_2 (round).

The XRD diffractogram collected for SiC04 foam (fig.6, left) is characteristic of a α -SiC phase (triangle) Moissanite-6H, JCPDF 74-1302, Hexagonal system, P63mc space group (186)). The Si peaks (square) provide from infiltrated Si in the SiC compound.(JCPDF 71-4631, cubic system, Fd-3m space group (227)).

For heated SiC04 foam, minor SiO_2 phase (round) was detected (alpha low cristobalite, JCPDF 76-0941, tetragonal system, P41212 space group (92)). The surface of the SiC foam was oxidised. Si preferential orientations in the (200) direction (virgin) and (311) direction (heated sample) were observed.

The XRD patterns collected for SiC05 foams (fig.7, right) are characteristic of a β -SiC phase (Moissanite-3C, JCPDF 73-1665, cubic system, F-43m space group (216)).

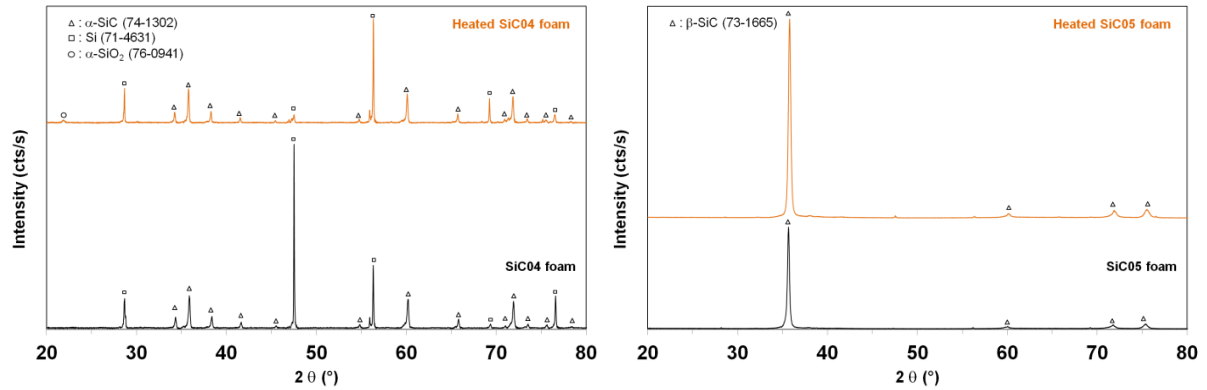


Figure 6: Diffraction patterns collected for no-heated and heated sample SiC04: α -SiC (triangle), α -SiO₂ (round) and Si (square)

Figure 7: Diffraction patterns collected for no-heated and heated sample SiC05: β -SiC (triangle)

The XRD patterns collected for initial and heated ZrB₂ samples are shown in figure 8. The diffractogram collected for ZrB₂ foam is attributed to a ZrB₂ phase (cross), (JCPDF 89-3930, Hexagonal system, P6/mmm space group (191)).

The purple and the green diffractograms were collected at the front face and inside the heated ZrB₂ foam, respectively. A minor ZrO₂ phase (full round) was detected (JCPDF 83-0940, monoclinic system, P21/c space group (14)).

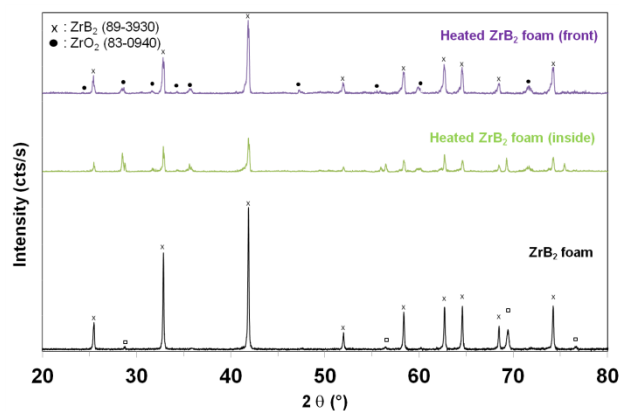


Figure 8: Diffraction patterns collected for no-heated and heated ZrB₂ foams (front side: purple and inside: green): ZrB₂ (cross), ZrO₂ (full round) and Si (square)

Discussion:

The XRD analyses were carried out in order to observe the modifications of crystalline phases after the heating treatment and to estimate the chemical and the crystallinity quality of foams.

For Al₂O₃ and ZrO₂ foams, no significant modifications of the peak intensities were observed between original and heated diffractograms. These features are composed by several splitting peaks and shoulders for the same crystalline phase. All these results indicate a low-quality crystallinity of the Al₂O₃ and ZrO₂ foams. According to other studies⁽¹⁾,



similar properties of reflectance and absorptivity were observed for shorter solar wavelengths (under 3 μm). The solar absorptivity values are not interesting, in the range of 0.25 to 0.4⁽⁶⁹⁻⁷²⁾. Low efficiency for thermal solar conversion was calculated⁽²⁾.

Two oxide phases of silica and zirconia were detected for virgin SiC02-03 samples. The virgin and heated samples show low-quality crystallinity. According to previous results⁽²⁾, the total absorptivity and efficiency of the material decrease with increasing the quantity of SiO₂ ($\alpha=0.10-0.15$) or/and Al₂O₃ ($\alpha=0.3-0.4$) compounds^(69,71,73-75) in the SiC layer.

The SiC01, 04 and 05 samples revealed high-quality crystallinity and promising efficiency values (82-83 %) for absorber applications. The absorptivity values measured for pure SiC foams are close to $\alpha=0.7-0.8$ (IR-TF SOC 100 device). A minor crystalline phase of α -SiO₂ was only detected for SiC01 and SiC04 heated foams. However, the cavity size of the SiC01 sample is small (40 PPI) for spectroscopic and electronics analysis technique (electron scattering effects in the cavity walls, source size...). For sample SiC04, the presence of Si indicates a thin SiC layer and/or included Si in the SiC layer. It is more sensitive to an oxidation process than sample SiC05 (fig.6 and 7). In comparison with sample SiC05, previous XPS results show the presence of a SiO₂ layer at the surface of the virgin α -SiC (SiC04) (fig.9 and table 4). The measured thickness of this oxide layer is about 20 nm (XPS depth profile).

Sample	Atomic compositions (%)			
	C	N	O	Si
SiC04	/	/	58.2	42.8
SiC05	43.8	5.3	3.7	47.2

Table 4: Atomic compositions (%) measured from the C 1s, N 1s, O 1s and Si 2p_{1/2,3/2} spectra collected for virgin SiC samples (SiC04 and SiC05).

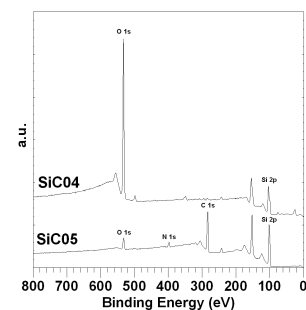


Figure 9 (right): XPS spectra collected for virgin SiC samples: SiC04 and SiC05

The ZrB₂ sample revealed high-quality crystallinity. A minor ZrO₂ phase was detected. The amount of zirconia is more important for the diffractogram collected inside the foam. During the heating treatment, the temperature is higher inside the ceramic foam. This sample presents promising efficiency values (83 %) for absorber applications⁽⁷⁶⁾.

According to these results and discussion, the selected samples for XPS analysis are SiC05 and ZrB₂.

5) Results and discussion: XPS analysis



The XPS analyses were carried out in order to determine the chemical environment, the nature of the chemical bonds, and the chemical composition from the surface to the substrate for heated samples.

The technical challenge was to select a set parameter of high voltage, current intensity, beam size (X-ray source, ion and flood guns...) to analyze no-flat and rough surfaces or wall in a cavity. The experimental conditions were optimized in order to eliminate or reduce the electrons effects (backscattering and scattering phenomena). Etching parameters were fixed (Ei, ion flux...) using determined sputtering indicators leading to correct sputter rate or relative sputter yield and atomic composition accuracy in depth.

For example, optimized depth profiling conditions were determined from reference CVD β -SiC sample in order to having the expected efficiency (fig. 10) of the sputtering process taking to account the ion beam effects or damages (fig.11) (13,77): The rate of induced Si-Si bonds was also observed.

In summary, for XPS analyses of near-surface, the ion sputtering time and the ion flux were limited to 10 s and $1.25 \cdot 10^{-22}$ ions/cm², respectively.

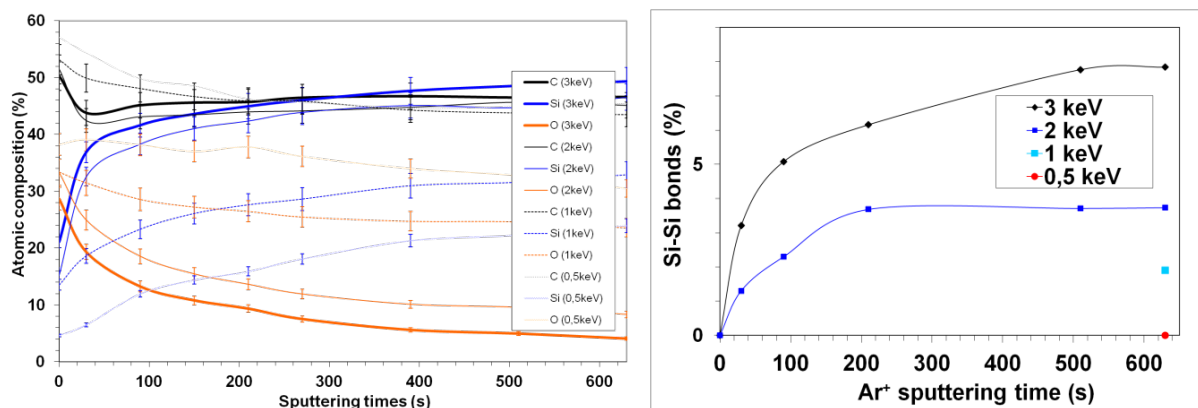


Figure 10 (left): Evolution of chemical compositions versus sputtering time at different ion energies: reference CVD β -SiC

Figure 11 (right): Evolution of new species induced by ion sputtering (Si-Si bonds): reference CVD β -SiC

5.1) Qualitative and quantitative depth profiles (SiC foam)

Some results of atomic compositions (%) collected during XPS depth profiles (SiC05) are shown in table 1 - figure 12 (front face) and table 2 –figure 13 (back face). The front face of the foam is the irradiated surface by solar flux. The atomic compositions were measured based on C 1s, O 1s and Si 2p_{1/2,3/2} core level photoelectron peaks.

Sample SiC05 (ff):	Atomic compositions (%)		
Sputtering times (s)	C	O	Si

Sample SiC05 (bf):	Atomic compositions (%)		
Sputtering times (s)	C	O	Si



0	15.8	45.3	38.9	0	8.1	48.9	43.0
60	1.1	63.5	35.4	60	14.1	43.4	42.5
100	1.5	62.6	35.9	100	18.8	37.1	44.1
200	8.4	52.1	39.5	200	22.9	28.4	48.7
600	33.2	14.3	52.5	600	34.5	15.2	50.3
1600	46.1	3.1	50.8	1600	43.5	5.2	51.3
ASF	1	2.9	0.79	ASF	1	2.9	0.79

Table 5 (left): Some atomic compositions (%) measured from the C 1s, O 1s, Si 2p_{1/2,3/2} XPS spectra (front face, SiC05).

Table 6 (right): Some atomic compositions (%) measured from the C 1s, O 1s, Si 2p_{1/2,3/2} XPS spectra (back face, SiC05).

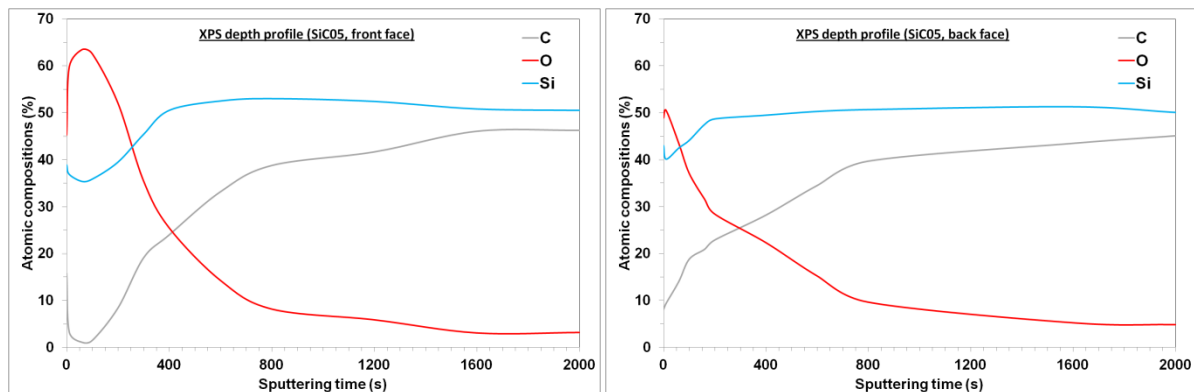


Figure 12 (left): Evolution of the atomic compositions (%): XPS depth profile collected for sample SiC05 on front side (ff)

Figure 13 (right): Evolution of the atomic compositions (%): XPS depth profile collected for sample SiC05 on back side (bf)

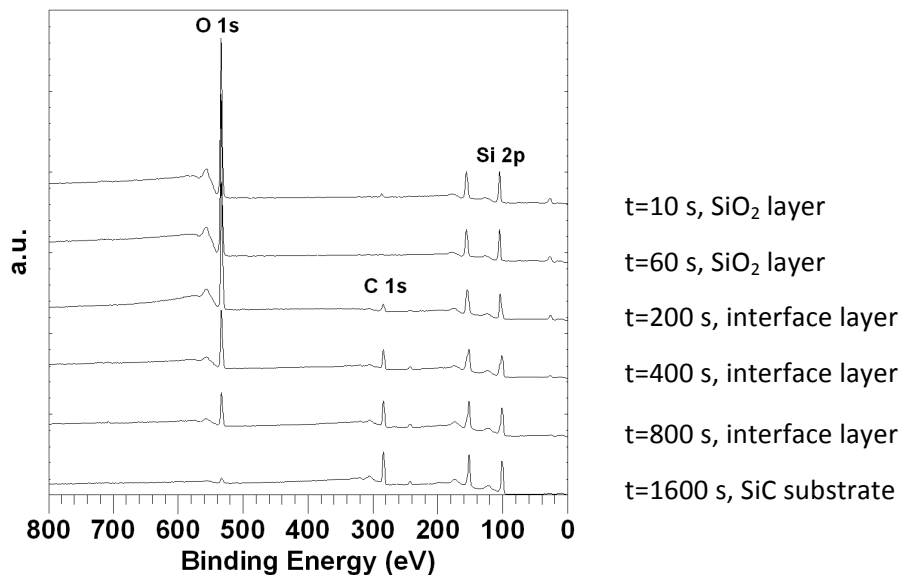


Figure 14: XPS depth profile collected for sample SiC05 on front side (ff)

On the front side surface (table 5, fig. 12 and 14) the presence of adventitious carbon species at the surface (t=0 s) is due to atmospheric contaminant species (hydrocarbon). These species were removed after 10 s of sputtering process. In the range of t=0 to 100 s of sputtering times (SiC05 (ff)), the calculated O/Si ratio is close to 1.8. The silica layer seems to be homogenous and its calculated thickness is about 15 ± 4 nm. The SiC surface is fully



oxidized. The interface layer is clearly defined and the measured thickness is less than 10 nm. The substrate of SiC was reached after 350 s of sputtering time. The residual oxygen amount provide from oxygen re-deposition species from no-cleaned surfaces. 2 layers were clearly identified from surface to the SiC substrate: a homogenous SiO₂ and an interface layer.

On the back side surface (table 6, fig. 13), after 10 s of sputtering time, no homogenous silica layer was clearly observed. Si, C and O element are all measured in various quantities. Oxide silicon and SiC compounds are both detected. These results indicate the presence of oxidized and no-oxidized surfaces rather than a continuous interface layer. The amount of O slowly decreases because of the presence of a more important roughness of surface. Two compounds were identified: silica (oxidized substrate) and SiC (not oxidized substrate).

The assignment of the C 1s, O 1s, and Si 2p_{1/2,3/2} components from the XPS spectra collected for the SiC05 (ff) and SiC05 (bf) compounds is summarized in Table 7.

Main components positions, FWHM, nature of the chemical bonds and compounds					
O 1s		Si 2p _{1/2,3/2}		C 1s	
532.8	103.4	102.0	100.5	285.3	282.8-283.0
(1.8)	(1.7)	(1.8)	(1.4)	(1.5)	(1.3)
O-Si	Si-O	Si-O-C	Si-C	C-O/C-C	Si-C
SiO ₂	SiO ₂	SiO _x C _y	SiC	hydrocarbon	SiC

Table 7: Main components positions (± 0.1 eV), FWHM (± 0.05 eV), chemical bonds and related compounds: C 1s, O 1s and Si 2p_{1/2,3/2} photoelectron peaks of SiC05 (ff, bf).

The Si 2p_{1/2,3/2} spectra of samples SiC05 (ff) and (bf) (Fig. 15 and 16) were curve fitted with 1 to 3 components. The C 1s and O 1s spectra were not shown.

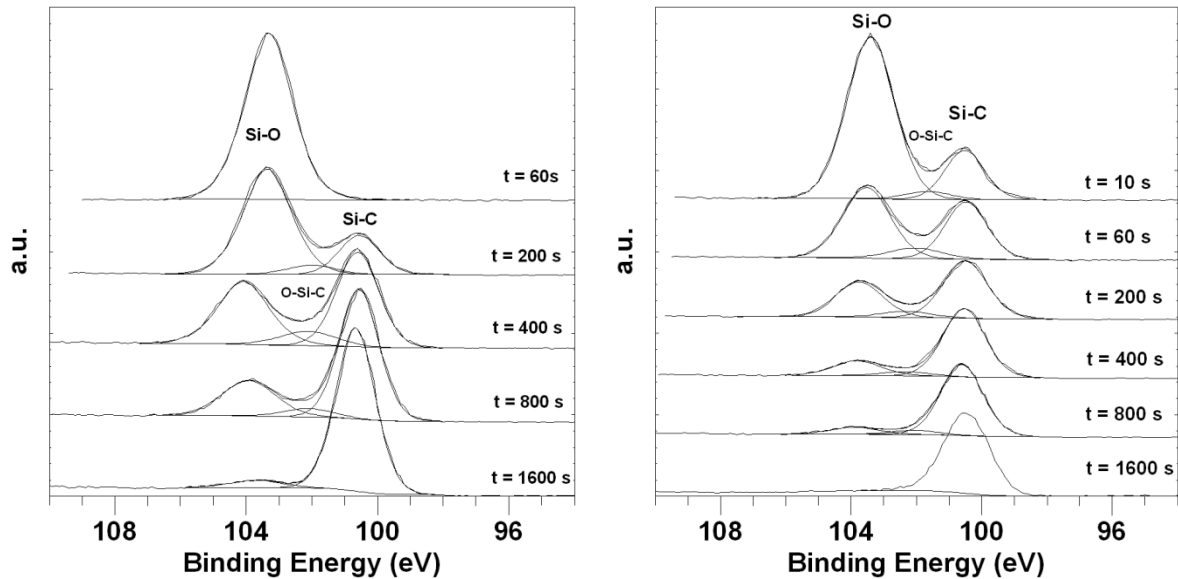


Figure 15: Depth profile of Si $2p_{1/2,3/2}$ photoelectron peaks collected for sample SiC05 (ff)

Figure 16: Depth profile of Si $2p_{1/2,3/2}$ photoelectron peaks collected for sample SiC05 (bf)

The components located at 100.5 ± 0.1 eV and 282.8 ± 0.1 eV are attributed to Si–C or C–Si bonds in a SiC compound (no oxidized substrate).

The components detected at 103.2 ± 0.1 eV and 532.8 ± 0.1 eV are attributed to Si–O or O–Si bonds in SiO_2 (silica, oxidized substrate).

The components detected at 102.0 ± 0.1 eV are attributed to mixed C–Si–O bonds in SiO_xC_y compounds ($x + y = 4$).

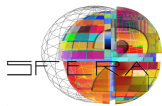
These XPS results are in good agreement with others works on SiC oxidation^(13,46,78-84) or reference databases⁽⁸⁵⁻⁸⁷⁾.

Discussion:

The shift between the O–Si and O–C component is less than 0.3 eV. Thus, in the peak-fitting process, only one component (532.4 ± 0.1 eV) was used to identify these two types of bonds (O–C and O–Si)^(58,78).

At $t=10$ s and 60 s (sample SiC05 (bf)) the Si-C component (fig. 15-16) is already detected in comparison with sample SiC05 (ff). This result shows the presence of SiO_2 and SiC compounds and an imperfect oxidation process of SiC substrate^(46,58).

The presence of Si-O-C mixed bonds induced chemical shifts of components between 100.5 to 103.2 eV (Si 2p photoelectron peaks). Only one component (rather than three components corresponding to Si-OC_3 , $\text{Si-O}_2\text{C}_2$ and $\text{Si-O}_3\text{C}$ chemical environment) was added in the Si 2p, with a higher FWHM. The goal is to determine the main chemical environment at the interface zone. According to previous works^(46,80,88) and other authors^(79,81,83,84,89-94), the interface is mainly composed by SiO_2C_2 chemical environments.



Despite an optimization of ion effects, intermediary compounds could be formed due to possible silica reduction during the sputtering process. These compounds could be present in the O-Si-C components (fig.15-16). However, no component characteristic of Si-Si bonds (99.5 ± 0.1 eV) was detected⁽⁹⁵⁻⁹⁸⁾ (Ar⁺ etching effects).

On front side of sample SiC05, the Si-O bonds are the preponderant contributions on the surface due to the formation of silica. The quantities of Si-O bonds and O-Si bonds increase with increasing the oxidation temperature. A homogenous and protective SiO₂ layer covers the SiC substrate. SiO_xC_y chemical environment are identified as interface compounds.

On back side, a contribution of Si-C and C-Si bonds is detected on surface. For active oxidation, the amount of Si-C bonds and C-Si bonds increases with increasing the annealing temperature due to the presence of mainly SiC on the surface. However, on the back side surface the presence of Si-C bonds is not due to an active oxidation behavior but only due to a lower surface temperature (1200 K) leading to an incomplete oxidation of the foam surface. Only one part of the detected SiC substrate was oxidized. So, the amount of SiO_xC_y compounds is lower on back face than on front face.

5.2) Qualitative and quantitative depth profiles (ZrB₂ foam)

XPS depth profile collected for sample ZrB₂ (ff) is shown on figures 17 and 18. The front face of the foam is the irradiated surface by solar flux. The atomic compositions (table 8) were measured based on N 1s, B 1s, O 1s and Si 2p_{1/2,3/2} core level photoelectron peaks.

Sample ZrB2 (ff):	Atomic compositions (%)			
Sputtering times (s)	N	B	O	Si
10	9.3	15.4	48.4	26.9
200	8.4	16.7	48.5	26.4
1200	7.4	15.6	54.9	22.1
ASF	1.8	0.49	2.9	0.79

Table 8: Some atomic compositions (%) measured from the N 1s, B 1s, O 1s and Si 2p_{1/2,3/2} XPS spectra (front face, ZrB₂).

The adventitious carbon species due to atmospheric contaminant species (hydrocarbon) were removed after 10 s of sputtering process. In the range of t=0 to 1800 s of sputtering times (ZrB₂ (ff)), one homogenous layer was identified. However, Zr atoms were not detected. An oxidized layer is probably composed by O, Si and B atoms. The ZrB₂ substrate was not reached after 1800 s of sputtering time.

On the surface spectra of ZrB₂ (bf)), Si, O and Zr elements were only detected.

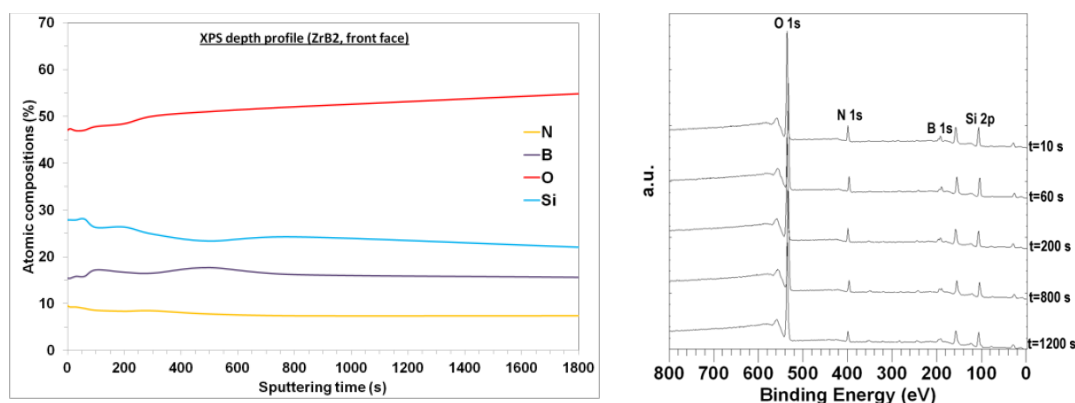


Figure 17 (left): Evolution of the atomic compositions (%): XPS depth profile collected for sample ZrB₂ on front side (ff)

Figure 18 (right): Some XPS spectra collected for sample ZrB₂ (ff): XPS depth profile

The assignment of the B 1s, N 1s, O 1s and Si 2p_{1/2,3/2} components from the XPS spectra collected for sample ZrB₂ (ff) is summarized in Table 9.

Main components positions, FWHM, nature of the chemical bonds and compounds				
B 1s		N 1s	O 1s	Si 2p _{1/2,3/2}
193.4	190.6	396.8	532.8	103.3
(2.3)	(1.8)	(1.8)	(2.1)	(2.3)
O-B	N-B	N-B	O-Si	Si-O
B ₂ O ₃	BN	BN	SiO ₂ , B ₂ O ₃	SiO ₂

Table 9: Main components positions (± 0.1 eV), FWHM (± 0.05 eV), chemical bonds and related compounds: B 1s, N 1s, O 1s and Si 2p_{1/2,3/2} photoelectron peaks of ZrB₂ (ff).

The two components of the B 1s spectrum (fig.19) located at 190.6 ± 0.1 eV and 193.4 ± 0.1 eV were attributed to B-N and B-O bonds. No B-Zr bonds (187.8 ± 0.1 eV, ZrB₂ substrate) were detected. On the same figure, no Zr 3d_{5/2} and Zr 3d_{3/2} peaks were observed.

The N 1s spectrum was mainly curve fitted with one component located at 396.8 ± 0.1 eV. This component could be attributed to N-B bonds.

The components detected at 103.3 ± 0.1 eV (fig. 21) and 532.8 ± 0.1 eV (fig. 22) are attributed to Si-O and O-Si bonds in SiO₂ (silica). Higher FWHM for these components could indicate the presence of mixed bonds or chemical environments (B-O-Si).

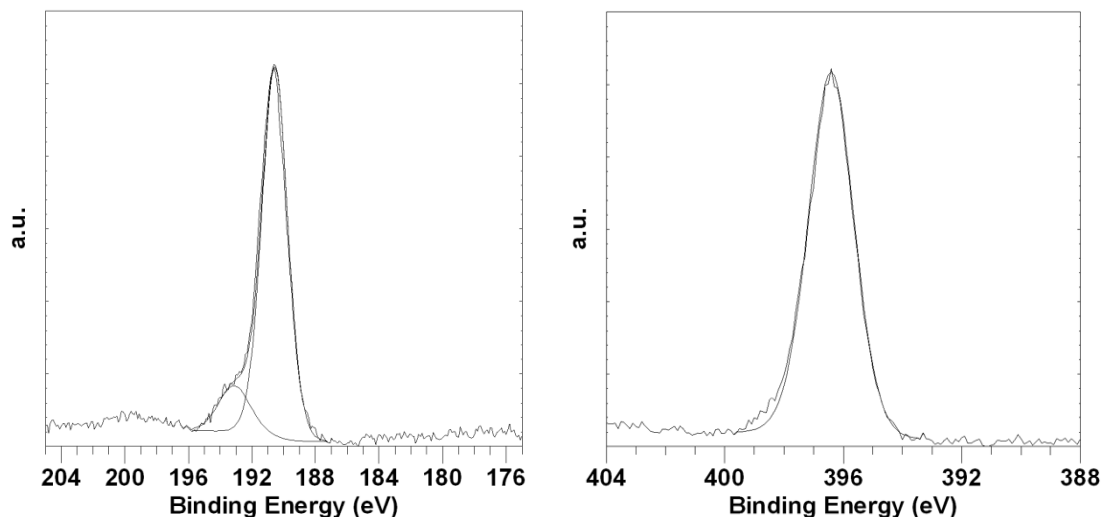


Figure 19 (left): B 1s photoelectron peak collected for sample ZrB₂ (ff)

Figure 20 (right): N 1s photoelectron peak collected for sample ZrB₂ (ff)

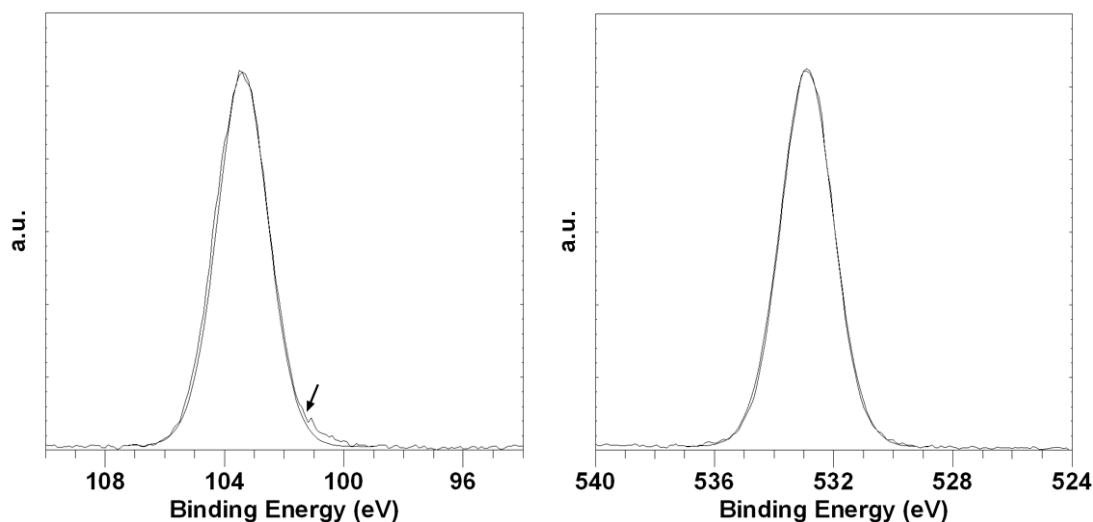


Figure 21 (left): Si 2p_{1/2,3/2} photoelectron peak collected for sample ZrB₂ (ff)

Figure 22 (right): O 1s photoelectron peak collected for sample ZrB₂ (ff)

These XPS results are in good agreement with our previous studies^(58,99) and with other works on ZrB₂ oxidation⁽¹⁰⁰⁻¹⁰²⁾ or reference databases⁽⁸⁵⁻⁸⁷⁾.

Discussion:

The surface chemical composition of sample ZrB₂ (ff) shows a SiO₂-rich layer. Based on the value of the relative vapour pressure of B₂O₃(l) and SiO₂(l), B₂O₃(l) compound must be preferentially evaporated. Si species moved through the Si-ZrB₂ layer to form a mixed ZrO₂(s)-SiO₂(l) layer, first. SiO₂(l) compound would be above the ZrO₂(s)-SiO₂(l) mixed layer and was crystallized in a SiO₂(s) compound on the surface during the cooling process.

The BN compound was formed by the reaction with N₂ (air flux) with the dissociated B₂O₃ compounds at high temperature (1900 K). No boron nitride was detected on back face



of the ZrB_2 (bf)). The presence of BN compounds at high temperature was studied by Bois et al.⁽¹⁰³⁾. B-N bonds are formed by B-O bond cleavage above 1400 K and a pyrolysis process up to 2000 K leads to a partial crystallization of hexagonal BN. No mixed compound (SiBNO: boro-silicon oxynitride) was clearly observed on the ZrB_2 (ff) spectra. The XPS-spectra corresponding to this compound is a Si 2p component located at about 102.2 ± 0.1 eV. However, the component of the B 1s spectrum shift to 193.2 (-0.4 eV) and higher FWHM of the Si 2p spectra was observed, indicating the presence of a small amount of mixed chemical bonds (SiOB). Above 1700 K, the rate of vaporization of B_2O_3 is higher than the rate of its formation. However, boria can be detected within the oxide layer^(52,63). Several studies revealed high oxidation resistance up to 1800 K. A protective layer of borosilicate compound was formed at the surface. The vaporization of B_2O_3 is stopped and boria compound is enclosed in a borosilicate glass which presents higher melting temperature and lower oxygen diffusion than the B_2O_3 glass^(49,54,57-59,63,64,104,105).

Above 1800 K, phase diagrams suggest the presence of stable $ZrSiO_4$ compound^(104,106). However, our work does not report the formation of significant or detectable amounts of $ZrSiO_4$ compound in good agreement with other oxidation studies^(49,58,107).

6) Conclusions

This study concerns the characterization of the surface cavities of porous materials as ceramics foams used in high temperature volumetric solar absorbers. SEM and ATG techniques are usually used for their analyses. Experimental methods (XRD, XPS) were optimized (source size, surface, bulk, geometric and sources effects...) in order to characterize the microstructure of the pore walls. XPS is one of the most promising and appropriate techniques to analyze oxidized foams (surface and bulk informations). After a heating treatment with solar energy, the microstructure (crystalline phases, chemical bonds and environments, chemical composition...) and the oxidation behavior of the ZrB_2 and SiC foams were determined. These techniques can be performed for aging tests in our laboratory.



Figures caption:

Figure 1: 6 kW solar furnace experimental setup Figure 2: Solar reactor device (OPTISOL) ⁽²⁾ 8

Figure 3: Diffraction patterns collected for no-heated and heated Al₂O₃ (3a) and ZrO₂ (3b) foams. ... 10

Figure 4 (left): Diffraction patterns collected for no-heated and heated sample SiC01: α-SiC (triangle), α-SiO₂ (round) and Si (square) 11

Figure 5 (right): Diffraction patterns collected for no-heated and heated sample SiC02: α-SiC (triangle), Al₂O₃ (diamond) and α-SiO₂ (round). 11

Figure 6: Diffraction patterns collected for no-heated and heated sample SiC04: α-SiC (triangle), α-SiO₂ (round) and Si (square) 12

Figure 7: Diffraction patterns collected for no-heated and heated sample SiC05: β-SiC (triangle) 12

Figure 8: Diffraction patterns collected for no-heated and heated ZrB₂ foams (front side: purple and inside: green): ZrB₂ (cross), ZrO₂ (full round) and Si (square)..... 12

Figure 9 (right): XPS spectra collected for virgin SiC samples: SiC04 and SiC05..... 13

Figure 10 (left): Evolution of chemical compositions versus sputtering time at different ion energies: reference CVD β-SiC 14

Figure 11 (right): Evolution of new species induced by ion sputtering (Si-Si bonds): reference CVD β-SiC 14

Figure 12 (left): Evolution of the atomic compositions (%): XPS depth profile collected for sample SiC05 on front side (ff) 15

Figure 13 (right): Evolution of the atomic compositions (%): XPS depth profile collected for sample SiC05 on back side (bf) 15

Figure 14: XPS depth profile collected for sample SiC05 on front side (ff) 15

Figure 15: Depth profile of Si 2p_{1/2,3/2} photoelectron peaks collected for sample SiC05 (ff) 17

Figure 16: Depth profile of Si 2p_{1/2,3/2} photoelectron peaks collected for sample SiC05 (bf) 17

Figure 17 (left): Evolution of the atomic compositions (%): XPS depth profile collected for sample ZrB₂ on front side (ff)..... 19

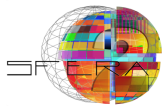
Figure 18 (right): Some XPS spectra collected for sample ZrB₂ (ff): XPS depth profile..... 19

Figure 19 (left): B 1s photoelectron peak collected for sample ZrB₂ (ff) 20

Figure 20 (right): N 1s photoelectron peak collected for sample ZrB₂ (ff) 20

Figure 21 (left): Si 2p_{1/2,3/2} photoelectron peak collected for sample ZrB₂ (ff)..... 20

Figure 22 (right): O 1s photoelectron peak collected for sample ZrB₂ (ff) 20



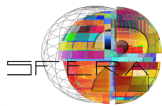
Tables caption:

Table 1: Identification of the ceramic foams	9
Table 2: Identification of the ceramic foams: Al ₂ O ₃ , ZrO ₂ , SiC01, SiC02, SiC03.....	9
Table 3: Identification of the ceramic foams (EngiCer manufacturer): SiC04, SiC05, ZrB ₂	10
Table 4: Atomic compositions (%) measured from the C 1s, N 1s, O 1s and Si 2p _{1/2,3/2}	13
Table 5 (left): Some atomic compositions (%) measured from the C 1s, O 1s, Si 2p _{1/2,3/2} XPS spectra (front face, SiC05).	15
Table 6 (right): Some atomic compositions (%) measured from the C 1s, O 1s, Si 2p _{1/2,3/2} XPS spectra (back face, SiC05).	15
Table 7: Main components positions (± 0.1 eV), FWHM (± 0.05 eV), chemical bonds and related compounds: C 1s, O 1s and Si 2p _{1/2,3/2} photoelectron peaks of SiC05 (ff, bf).	16
Table 8: Some atomic compositions (%) measured from the N 1s, B 1s, O 1s and Si 2p _{1/2,3/2} XPS spectra (front face, ZrB ₂).....	18
Table 9: Main components positions (± 0.1 eV), FWHM (± 0.05 eV), chemical bonds and related compounds: B 1s, N 1s, O 1s and Si 2p _{1/2,3/2} photoelectron peaks of ZrB ₂ (ff).	19

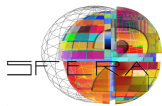


7) References

1. E. Sani, L. Mercatelli, J.L. Sans, D. Sciti. *Sol. Energy mater. Sol. cells.* 20015, Vol. 140, pp. pp. 477-482.
2. S. Mey-Cloutier, C. Caliot, A. Kribus, Y. Gray, G. Flamant. *Solar Energy.* 2016, Vol. 136, pp. pp. 226-235.
3. G. Harris. *Properties of silicon carbide.* London: INPEC, 1995. Vol. 13.
4. K.G. Nickel, J. Desmaison. *J. Eur. Ceram. Soc.* 2005, Vol. 25, pp 1697-1818.
5. D.E. Rosner, H.D. Allendorf. *J. Phys. Chem.* 1970, Vol. 74, pp 1829-1839.
6. E.A. Gulbransen, S.A. Jansson. *Oxid. Metals.* 1972, Vol. 4, pp 181-201.
7. T. Narushima, T. Goto, Y. Iguchi, T. Hirai. *J. Am. Ceram. Soc.* 1991, Vol. 74, pp 2583-2586.
8. M.J.H. Balat. *J. Eur. Ceram. Soc.* 1996, Vol. 16, pp 55-62.
9. H. Hatta, T. Aoki, Y. Kogo, T. Yarii. *Composites: Part A.* 1999, pp 515-520.
10. T. Sekigawa, K. Oguri, J. Kochiyama, K. Miho. *Mater. Trans.* 2001, Vol. 42, pp 825-828.
11. T. Ogasawara, T. Aoki, M. Sayed Aly Hassan, Y. Mizokami, N. Watanabe. *Composites: Part A.* 2011, pp. 221-228.
12. L. Charpentier, M. Balat-Pichelin, F. Audubert. *J. Eur. Ceram. Soc.* 2010, Vol. 30, pp. 2630-2660.
13. L. Charpentier, M. Balat-Pichelin, H. Glénat, E. Bêche, E. Laborde, F. Audubert. *J. Eur. Ceram. Soc.* 2010, pp. 2661-2670.
14. K. Dawi, M. Balat-Pichelin, L. Charpentier, F. Audubert. *J. Eur. Ceram. Soc.* 2012, Vol. 32, pp. 458-494.
15. E.J. Opila. *J. Am. Ceram. Soc.* 1995, Vol. 78, p. 1107.
16. —. *J. Am. Ceram. Soc.* 1997, Vol. 80, p. 197.
17. —. *J. Am. Ceram. Soc.* 1994, Vol. 77, p. 730.
18. L.U.J.T. Ogbuji, E.J. Opila. *J. Electrochem. Soc.* 1995, Vol. 14, p. 925.
19. Z. Zheng, R. E. Tressler, K.E. Spear. *J. Electrochem Soc.* 1990, Vol. 137, p. 850.
20. C. Virojanadara, L. I. Johansson,. *Surf. Sci.* 2002, Vol. 519, p. 73.
21. M. Kildemo, U. Grossner, M. Juel, B. G. Svensson, S. Raaen,. *Surf. Sci.* 2006, Vol. 600, p. 1300.
22. K. Krnel, D. Sciti, E. Landi, A. Bellosi,. *Appl. Surf. Sci.* 2003, Vol. 210, p. 274.
23. C. E. Ramberg, W. L. Worrell,. *J. Am. Ceram. Soc.* 2001, Vol. 84, p. 2607.
24. T. Narushima, T Goto, T. Hirai. *J. Am. Ceram. Soc.* 1989, Vol. 72, p. 1386.
25. W. Hinze, H. C. Graham. *J. Electrochem. Soc.* 1976, Vol. 123, p. 1066.
26. C. E. Ramberg, G. Cruciani, K. E. Spear, R.E. Tressler, C. F. Ramberg. *J. Am. Ceram. Soc.* 1996, Vol. 79, p. 730.
27. L. U. J. T. Ogbuji. *J. Am. Ceram. Soc.* 1997, Vol. 80, p. 1544.
28. W. L. Vaughn, H. G. Maahs,. *J. Am. Ceram. Soc.* 1990, Vol. 73, p. 1540.
29. K.G. Nickel. *J. Eu. Ceram. Soc.* 1992, Vol. 9, p. 3.
30. B. Schneider. *J. Mater. Sci.* 1998, Vol. 33, p. 535.
31. J. Wang, L. Zhang, Q. Zeng, G. Vignoles, A. Guette,. *J. Am. Ceram. Soc.* 2008, Vol. 91, p. 1665.
32. Y. Song, S. Dhar, L. C. Feldman, G. Chung, J. R. Williams,. *J. Appl. Phys.* 2004, Vol. 95, p. 4953.
33. S. R. Shah, A. Saha and R. Raj,. *J. Am. Ceram. Soc.* 2003, Vol. 86, p. 351.
34. J. Roy, S. Chandra, S. Das, S. Maitra,. *Rev. Adv. Mater. Sci.* 2014, pp. 29-39.
35. N.S. Jacobson, D.L. Myers,. *Oxid. Metals.* 2011, Vol. 75, pp. 1-25.
36. E. Beche, R. Berjoan, G. Peraudeau, B. Armas, C. Combescure, F. Sibieude,. *Annual Report 1, Brite-Euram BE 96-3012 UHTHE.* 1997, pp. 80-95.
37. E. Beche, R. Berjoan, G. Peraudeau, B. Armas, C. Combescure, F. Sibieude. *Mid-Term Report 1, Brite-Euram BE 96-3012 UHTHE.* 1998, pp. 237-251.
38. D.M. Liu. *Ceram. Int.* 1997, Vol. 23, p. 620.
39. Y. Song, F.W. Smith,. *J. Am. Ceram. Soc.* 2005, Vol. 88, p. 1864.
40. M. Yoshimura, T. Ohji, K. Nihara,. *J. Am. Ceram. Soc.* 1997, Vol. 80, p. 797.
41. R. Vaben, D. Stover,. *J. Mater. Sci.* 1994, Vol. 29, p. 3791.
42. J. W. Fergus, W. L. Worrell,. *J. Am. Ceram. Soc.* 1995, Vol. 78, p. 1961.
43. D. Das, J. Farjas, P. Roura,. *J. Am. Ceram. Soc.* 2004, Vol. 87, p. 1301.
44. V. Presser, K.G. Nickel. *Crit. Rev. Solid State Mater. Sci.* 2008, pp. pp. 1–99.
45. Y. Ogura, T. Morimoto,. *Journal of the Electrochemical Society* 149, J47 (2002). *J. Electrochem. Soc.* 2002, Vol. 149.
46. J. Eck, M. Balat-Pichelin, L. Charpentier, E. Beche, F. Audubert,. *J. Eur. Ceram. Soc.* . 2008, Vol. 28, p. 2995.
47. C. Mroz. *Am. Ceram. Soc. Bull.* 1994, Vol. 73, 141-142.
48. W. G. Fahrenholtz, G. E. Hilmas, I. G. Talmy, J. A. Zaykoski,. *J. Am. Ceram. Soc.* 2007, Vol. 90, p. 1347.



49. F. Monteverde, A. Bellosi, J. Electrochem. Soc. 2003, Vol. 150, 11, pp. pp. B552-B559.
50. D. Sciti, M. Brach, A. Bellosi, Scripta Mater. 2003, Vol. 53, pp. pp. 1297–1302.
51. A. Rezaie, W.G. Fahrenholtz, G.E. Hilmas, J. Am. Ceram. Soc. 2006, Vol. 89, pp. pp. 3240-3245.
52. T.A. Parthasarathy, R.A. Rapp, M. Opeka, R.J. Kerans, Acta Mater. 2007, Vol. 55, pp. pp. 5999–6010.
53. W.M. Guo, G.J. Zhang, Y.M. Kan, P.L. Wang, J. of Alloys Compounds. 2009, Vol. 471, pp. pp. 502–506.
54. M.M. Opeka, I.G. Talmy, E.J. Wuchina, J.A. Zaykoski, S.J. Causey, J. Eur. Ceram. Soc. 1999, Vol. 19, pp. pp. 2405–2414.
55. M.M. Opeka, I.G. Talmy, J.A. Zaykoski, J. Mater. Sci. 2004, Vol. 39, pp. pp. 5887–5904.
56. E. Wuchina, M.M. Opeka, S. Causey, K. Buesking, J. Spain, A. Cull, J. Routbort, F. Guitierrez-Mora, J. Mater. Sci. 2004, Vol. 39, pp. pp. 5939–5949.
57. W.G. Fahrenholtz, J. Am. Ceram. Soc. 2005, Vol. 88, pp. pp. 3509–3512.
58. E. Beche, M. Balat-Pichelin, V. Flaud, J. Esvan, D. Sciti, D. Alfano, Surf. Interface Anal. 2014, Vol. 46, pp. pp. 817-822.
59. E.J. Opila, J. Smith, S.R. Levine, J. Lorinez, M. Reigel, Open Aerospace Engineering Journal. 2010, Vol. 3, pp. pp. 41-51.
60. E. Sani, M. Meucci, L. Mercatelli, D. Jafrancesco, J.L. Sans, L. Silvestroni, D. Sciti, J. Photonics Energy. 2014, Vol. 4, pp. pp. 045599-1,045599-8.
61. E. Randich, R.B. Pettit, Solar Energy. 1981, Vol. 5, 4, pp. pp. 425-434.
62. D. Sciti, L. Silvestroni, L. Mercatelli, J.L. Sans, E. Sani, Solar Energy Mat. Solar Cells. 2013, Vol. 109, pp. pp. 8-16.
63. I.G. Talmy, J.A. Zaykoski, M.M. Opela, J. Am. Ceram. Soc. 2008, Vol. 91, 7, pp. pp. 2250-2257.
64. W. G. Fahrenholtz, G. E. Hilmas, A. L. Chamberlain, J. W. Zimmermann, J. Mater. Sci. 2004, Vol. 39, 19, pp. pp. 5951-5957.
65. D. Sciti, M. Brach, A. Bellosi, Scripta Mater. 2005, Vol. 53, pp. pp. 1297-1302.
66. W.A. Rachinger, J. Sci. Instrum. 1948, Vol. 25, p. p. 248.
67. D.A. Shirley, Phys. Rev. B. 1972, Vol. 5, pp. pp. 4709-4714.
68. J.H. Scofield, J. of Elec. Spectros. and Related Phenom. 1976, Vol. 8, pp. pp. 129-137.
69. H. Moghadam, A. Samimi, A. Behzadmehr, Transp. Phenom. Nano Micro Scales. 2013, Vol. 1, pp. pp. 110-116.
70. J.H. Henninger, NASA Publication and Reports. 1984, Vol. 1121, pp. 1-46.
71. G. Hass, J.B. Ramsey, J.B. Heaney, J.J. Triolo, Appl. Optics. 1971, Vol. 10, 6, pp. pp. 1296-.
72. F. Cao, D. Kraemer, L. Tang, Y. Li, A.P. Litvinchuck, J. Bao, G. Chen, Z. Ren, Energy Environ. Sci. 2015, Vol. 8, pp. pp. 3040-3048.
73. G. Hass, J.B. Ramsey, J.B. Heaney, J.J. Triolo, Appl. Optics. 1969, Vol. 8, 2, pp. pp. 275-280.
74. A.P. Bradford, G. Hass, J.B. Heaney, J.J. Triolo, Appl. Optics. 1970, Vol. 9, 2, pp. pp. 339-344.
75. C.E. Kennedy, NREL. Golden, Colorado: s.n., 2002. pp. pp. 1-52. NREL/TP-520-31267.
76. A. Ambrosini, T.N. Lambert, C.L. Staiger, A.C. Hall, M. Bencomo, E.B. Stechel, SNL (sandia National Laboratory). Albuquerque, New Mexico: s.n., 2010. pp. pp. 1-41. SAND2010-7080.
77. V. Flaud, E. Beche, D. Perarnau, L. Charpentier, M. Balat-Pichelin, Fes (Morocco): s.n., 2010. ELSPEC 2010, May 03-06.
78. S. Scordo, M. Ducarroir, E. Bêche, R. Berjoan, J. Mater. Res. 1998, Vol. 13, p. pp. 3315.
79. M.S. Chandrasekar, N.R. Srinivasan, Ceram. Inter. 2016, Vol. 42, pp. pp. 8900-8908.
80. L. Charpentier, K. Dawi, M. Balat-Pichelin, E. Beche, F. Audubert, Corros. Sci. 2012, Vol. 59, pp. pp. 127-135.
81. A. Avila, I. Montero, L. Galan, J.M. Ripalda, R. Levy, J. Appl. Phys. 2001, Vol. 89, 1, pp. pp. 212-216.
82. X. Chen, L. Ning, Y. Wang, J. Li, X. Xu, X. Hu, M. Jiang, J. Mater. Sci. Technol. 2009, Vol. 25, 1, pp. pp. 115-118.
83. B. Hornetz, H.J. Michel, J. Halbritter, J. Mater. Res. 1994, Vol. 9, 12, pp. pp. 3088-3094.
84. K.H. Lee, S.K. Lee, K.S. Jeon, Appl. Surf. Sci. 2009, Vol. 255, pp. pp. 4414-4420.
85. M.P. Seah, Practical Surface Analysis. [éd.] M.P. Seah D. Briggs. 2nd edn. New-York: J. Wiley & Sons, 1993. Vol. 1.
86. J.F. Moulder, W.F. Stickle, P.E. Sobol, K.D. Bomben, Handbook of X-ray Photoelectron Spectroscopy. Eden Prairie: Perkin Elmer, Physical Electronics Division, 1995.
87. Alexander V. Naumkin, Anna Kraut-Vass, Stephen W. Gaarenstroom, Cedric J. Powell, National Institute of Standards and Technology (NIST). NIST X-ray Photoelectron Spectroscopy Database. [En ligne] June 2000. <http://srdata.nist.gov/xps/Default.aspx>.



88. **M. Reinholdt, A. Ilie, S. Roualdès, J. Frugier, M. Schieda, C. Coutanceau, S. Martemianov, V. Flaud, E. Beche, J. Durand.** *Membranes*. 2012, Vol. 2, pp. pp. 529-552.
89. **H.F. Li, S. Dimitrijević, D. Sweatman, H.B. Harrison, P. Tanner.** *J. Appl. Phys.* 1999, Vol. 86, 8, pp. pp. 4316-4321.
90. **M. Schurmann, S. Dreiner, U. Berges, C. Westphal.** *Phys. Rev. B*. 2006, Vol. 74, pp. pp. 035309-1 , 6.
91. **M.R. Alexander, R.D. Short, F.R. Jones, W. Michaeli, C.J. Blomfield.** *Appl. Surf. Sci.* 1999, Vol. 137, pp. pp. 179-183.
92. **R. Berjoan, E. Beche, D. Perarnau, S. Roualdes, J. Durand.** *J. Phys.IV*. 1999, Vol. 9, pp. pp. 1059-1068.
93. **G.M. Bancroft, H.W. Nesbitt, R. Ho, D.M. Shaw, J.S. Tse, M.C. Biesinger.** *Phys. Rev. B*. 2009, Vol. 80, pp. pp. 075405-1 - 075405-13.
94. **L.A. O'Hare, B. Parbhoo, S.R. Leadley.** *Surf. Interface Anal.* 2004, Vol. 36, pp. pp. 1427-1434.
95. **X. Wang, J. Xiang, W. Wang, J. Zhang, K. Han, H. Yang, X. Ma, C. Zhao, D. Chan, T. Ye.** *Appl. Phys. Lett.* 2013, Vol. 102, pp. pp. 041603-1 , 5.
96. **X. Wang, X. Yu, W. Yu, H. Feng, J. Wang, C. Yin, W. Lu, G. Fu.** *J. Mater. Sci.* 2014, Vol. 49, pp. pp. 1353-1358.
97. **K. Hirose, H. Nohira, K. Azuma, T. Hattori.** *Prog. Surf. Sci.* 2007, Vol. 82, pp. pp. 3-54.
98. **M. Imamura, N. Matsubayashi, J. Fan, M. Sasaki.** *Meas. Sci. Technol.* 2011, Vol. 22, pp. pp. 1-5.
99. **D. Alfano, L. Scatteia, F. Monteverde, E. Beche, M. Balat-Pichelin, J. Eur. Ceram. Soc.** 2010, Vol. 30, pp. pp. 2345-2349.
100. **D. Gao, Y. Zhang, J. Fu, C. Xu, Y. Song, X. Shi, Corros. Sci.** 2010, Vol. 52, p. pp. 3297.
101. **T. Aizawa, S. Hishita, S. Otani, Appl. Surf. Sci.** 2009, Vol. 256, p. pp. 1120.
102. **C. Monticelli, F. Zucchi, A. Pagnoni, M. Dal Colle, Electrochim. Acta.** 2005, Vol. 50, p. 3461.
103. **L. Bois, P. L'Haridon, X. Gouin, P. Grange, J.F. Létard, M. Birot, J.P. Pillot, J. Dunoguès. J. Alloys Compd.** 1996, Vol. 232, pp. pp. 244-253.
104. **W.G. Fahrenholtz. J. Am. Ceram. Soc.** 2007, Vol. 90, 1, pp. pp. 143-148.
105. **P.A. Williams, R. Sakidja, J.H. Perepsko, P. Ritt. J. Eur. Ceram. Soc.** 2012, Vol. 32, pp. pp. 3875-3883.
106. **E.M. Levin, C.R. Robbins, H.F. McMurdie. Phase diagrams for ceramists.** Columbus: American Ceramic Society, 1964. p. pp. 141. Vol. vol. 1.
107. **I.G. Talmy, J.A. Zaykoski, M.M. Opeka. Ceram. Eng. Sci. Proc.** 1998, Vol. 19, 3, pp. pp. 105-112.